

# Synergistic inhibition effect of Diantipyrylmethane and Potassium thiocyanate on mild steel corrosion in 1 M HCl solution

Kangquan Qiao, Ying Zeng\*

Chengdu University of Technology, College of Materials and Chemistry & Chemical Engineering, 1#, Dongsanlu, Erxianqiao, Chengdu 610059, Sichuan, P. R. China

\*E-mail: [hxsqiao@163.com](mailto:hxsqiao@163.com), [zengy@cdut.edu.cn](mailto:zengy@cdut.edu.cn)

*Received:* 9 April 2019 / *Accepted:* 29 May 2019 / *Published:* 30 June 2019

---

The inhibition effect of Diantipyrylmethane (DAM) and its synergistic effect with potassium thiocyanate (KSCN) on mild steel corrosion in 1 M HCl solution were investigated by electrochemical methods, gravimetric analysis and scanning electron microscopy (SEM). The experiment results show that the inhibition efficiency increases with the concentration of DAM alone and increases further with the presence of 2 mM KSCN. The synergism parameters demonstrate that DAM cation has a significant synergistic effect with thiocyanate anion, which is agree with the corresponding thermodynamic and kinetic parameters. The results of quantum chemical calculation confirm that the dication structure of DAM molecule in acid medium plays a vital role during corrosion inhibition of mild steel.

---

**Keywords:** Diantipyrylmethane, Potassium thiocyanate, Synergism, Steel corrosion

## 1. INTRODUCTION

Heterocyclic compounds are usually used as corrosion inhibitors to restrain acid corrosion of metals in different fields including oil-well acidizing, acid pickling, acid cleaning, etc [1-4]. These organic inhibitors may effectively absorb on metal surface and form protective barriers through heteroatoms and  $\pi$ -electrons of aromatic rings [5-6].

As an important heterocyclic compound, 4-[(1,5-dimethyl-3-oxo-2-phenylpyrazol-4-yl)methyl]-1,5-dimethyl-2-phenylpyrazol-3-one (DAM) molecule contains two conjugated pyrazolone rings and two phenyls, thus it exhibits certain inhibition ability for steel corrosion in H<sub>2</sub>SO<sub>4</sub> solution [7]. It is commonly observed that thiocyanate ion can enhance the adsorption ability of organic cations by forming interconnecting bridge between positive charged steel surface and organic cations in acid

medium [8-11]. In fact, some organic compounds including single pyrazolone ring have been found to be organic cations and have synergistic inhibition effect with thiocyanate ion on steel corrosion in acidic medium [12]. In this case, the inhibition ability of Diantipyrylmethane possessing two pyrazolone rings should be also improved with the addition of thiocyanate ions by bridging action, however, this research of the synergistic inhibition effect of Diantipyrylmethane and thiocyanate ion on steel corrosion in acidic medium has not been previously reported.

Hence, in this paper, the synergistic inhibition effect of DAM and thiocyanate ion on steel corrosion in 1 M HCl was investigated using weight loss, electrochemical measurements, SEM and quantum chemical calculation, as well as the calculated results relating to adsorption and corrosion process were discussed in detail.

## 2. EXPERIMENTAL

### 2.1 Material and sample preparation

The composition (wt %) of mild steel for tests is 0.14 % C, 0.19 % Si, 0.22 % Mn, 0.014 % P, 0.011% S, 0.05 % Cu and the rest is Fe. The dimensions of steel coupons used for surface analysis and weight loss test are 15 mm × 15 mm × 5 mm and 50 mm × 25 mm × 5 mm, respectively. The working area of steel electrode for electrochemical experiments is 1 cm<sup>2</sup>. Prior to each experiment, all steel surfaces were mechanically abraded using waterproof abrasive paper to 800 grit.

DAM (Shanghai Aladdin Biochemical Technology Co., Ltd), KSCN and Hydrochloric acid (36 %) were all of analytical grade. Prior to each test, the inhibitor solutions of DAM, KSCN and the mixture of DAM and KSCN were prepared in 1 M HCl solution separately.

### 2.2. Electrochemical measurements

Electrochemical workstation (PARSTAT2273, Princeton Applied Research) was applied for electrochemical experiments in a typical three-electrode system containing a platinum electrode, a saturated calomel electrode (SCE) and a steel electrode. Before starting each electrochemical measurement, the working surface of steel electrode was soaked in the test solution for 30 min to establish a steady open circuit potential (OCP). EIS tests were employed in the frequency range of 100 kHz to 10 mHz at OCP with the excitation signal amplitude of 5 mV, and EIS data were fitted and analyzed using an appropriate equivalent circuit by ZSimpWin software. The potentiodynamic polarization measurements were employed in the range of -250 to +250 mV (vs. OCP) at a scan rate of 0.5 mV/s, and the polarization data were fitted and analyzed using the extrapolation method. All measurements were implemented for three times to achieve the test reproducibility.

### 2.3. Weight loss measurements

Cleaned and weighed steel coupons were suspended and immersed in 1 M HCl solution without and with the investigated inhibitors for 6 h at various temperatures, separately. Then steel coupons were scrubbed by bristle brush, cleaned with distilled water and acetone, dried and weighed at

room temperature. All experiments were implemented in triplicate, and the average weight loss of the three steel coupons were calculated as results.

#### 2.4. SEM measurements

The surface morphology analysis of steel coupons after immersed in 1 M HCl solution with or not with the investigated inhibitors at 303K for 4 h were examined by SEM (Tescan Vega3, Czech Republic) at 25.0 kV.

#### 2.5. Calculation method

Quantum chemical calculation of DAM cation in aqueous phase was performed by Gaussian 09 program software. The B3LYP functional with 6-31G basis set was applied to optimize the molecular structure of organic cation and obtain the corresponding parameters by density functional theory (DFT).

### 3. RESULTS AND DISCUSSION

#### 3.1 Electrochemical impedance spectroscopy (EIS)

EIS tests were undertaken to analyze the inhibition behavior of DAM. The representative Nyquist and Bode plots of mild steel in 1 M HCl solution with different concentrations of DAM at 303 K are given in Fig. 1.

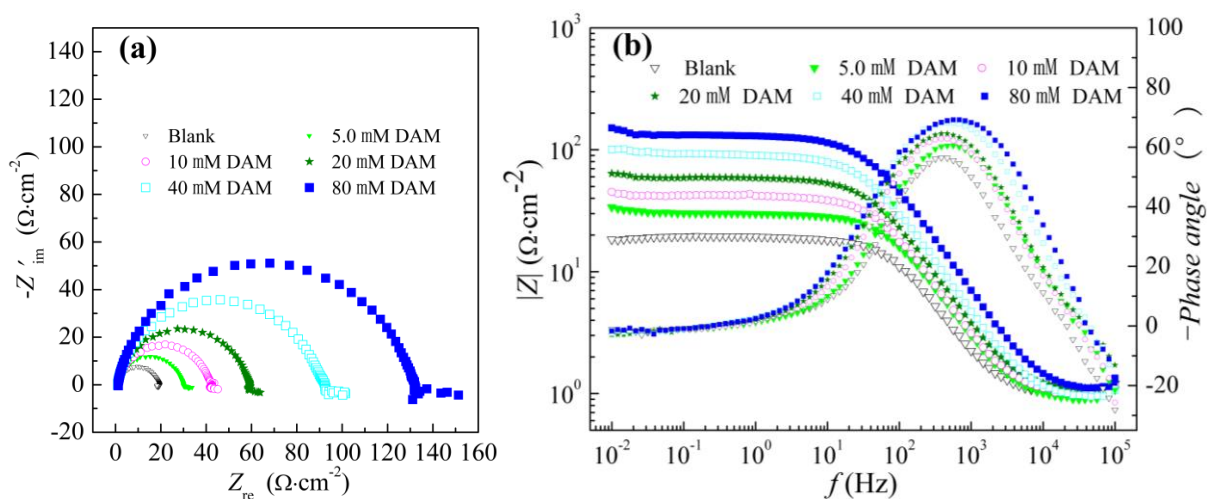


**Figure 1.** Nyquist (a) and Bode plots (b) of mild steel in 1 M HCl solution with different concentrations of DAM at 303 K

It is evident from Fig. 1 (a) that the diameters of capacitive loops at the high frequency (HF) distinctly improve with increasing DAM concentration, hinting that corrosion process is mainly controlled by charge-transfer [13]. Each Nyquist plot displays a depressed semicircular appearance, the deviation from ideal semicircle is generally due to the frequency dispersion and the nonuniformity of

corrosion surface [14]. The Nyquist plot in blank solution consists of a slight inductive loop at the low frequency (LF), however, the slight inductive loop completely disappears with the addition of DAM, indicating that DAM has some effect on the corrosion mechanism [15].

To study the synergistic inhibition effect of DAM and thiocyanate ion, Nyquist and Bode plots of steel in 1 M HCl and 2 mM KSCN solution with different DAM concentrations at 303 K were given in Fig. 2.

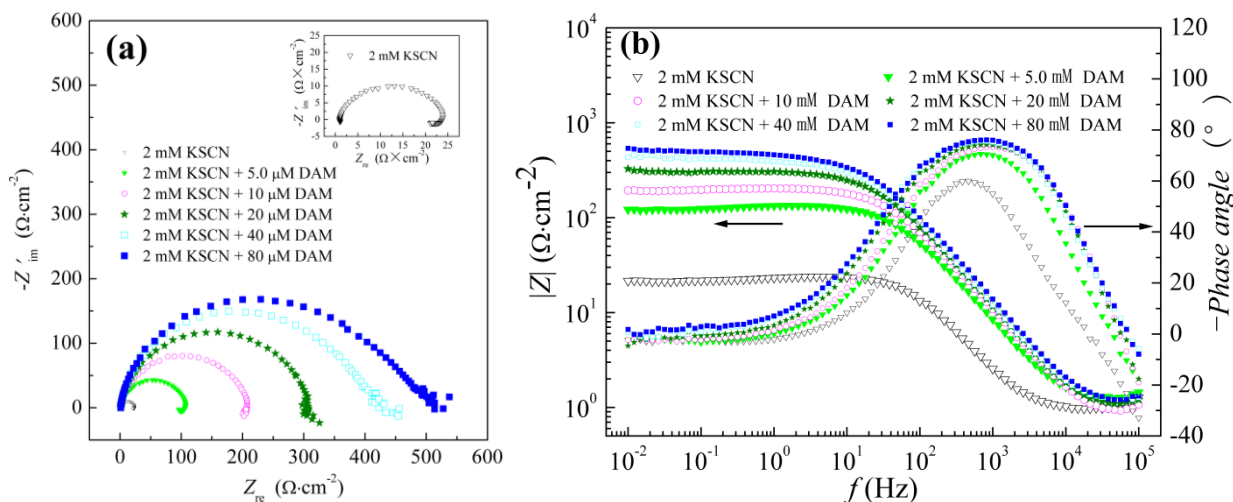


**Figure 2.** Nyquist and Bode plots of mild steel in 1 M HCl and 2 mM KSCN solution with different concentrations of DAM at 303 K

Similar to Fig. 1 (a), the diameters of the depressed capacitive loops at HF in Fig. 2 (a) also distinctly enhance with increasing DAM concentration. However, the diameters of capacitive loops at the same DAM concentration in Fig. 2 (a) are conspicuously larger than that in Fig. 1 (a), implying that the inhibition action of DAM can be dramatically improved with the addition of 2 mM KSCN. Nyquist plot of KSCN alone in LF consists of a distinct inductive loop, which is related to the relaxation process of the adsorption species on steel surface [15]. However, the LF inductive loop gradually degenerate with increasing DAM concentration in the presence of 2 mM KSCN, indicating that the change of corrosion inhibition mechanism coming from the influence of KSCN may be weakened by the addition of DAM. Obviously, Bode plots in Fig. 2 (b) and Fig. 1 (b) have similar shapes corresponding to one time constant [16,17].

To investigate the relation of EIS plots and the inhibition mechanism for steel corrosion in 1 M HCl solution, the equivalent circuit models in Fig. 3 were applied to fit EIS data by ZSimpWin software. Where  $R_s$  is the solution resistance,  $R_{ct}$  is the charge transfer resistance in accord with the diameter of Nyquist curve and the inhibition efficiency ( $\eta$ ), L and  $R_L$  are the inductive elements and CPE represents the constant phase element. The double layer capacitance ( $C_{dl}$ ) value can be influenced by the imperfections of steel surface, and this influence can be simulated by CPE. The  $C_{dl}$  value which may be calculated as follows [18-19]:

$$C_{dl} = Y_0(\omega_{max})^{n-1} = Y_0(2\pi f_{z_{im-max}})^{n-1} \tag{1}$$

where  $Y_0$  is the CPE constant,  $\omega_{max}$  in accord with  $f_{zim-max}$  is the maximum value of  $\omega$  at the imaginary part of Nyquist curve,  $n$  represents the phase shift which may quantify the different physical phenomena such as the surface roughness, the formation of porous layer and the adsorption of inhibitor molecules [20]. In general, the displacement of water molecules or other ions on steel surface/solution by inhibitor molecules may result in the decrease of the local dielectric constant and the  $C_{dl}$  value.

The  $\eta$  values may be calculated using the following equation [21-22]:

$$\eta \% = \frac{(R_{ct,0} - R_{ct,i})}{R_{ct,0}} \times 100 \% \tag{2}$$

where  $R_{ct,0}$  and  $R_{ct,i}$  are the  $R_{ct}$  values in the absence and presence of the investigated inhibitor respectively.

The extension of coverage degree of the inhibitor molecules absorbed on steel surface may commonly lead to the increase of the inhibition efficiency corresponding to  $R_{ct}$  value.

Base on the obtained  $\eta$  values, the synergism parameters ( $S$ ) may be calculated using the following equation [23-24]:

$$S = \frac{(1 - \eta_{DAM} - \eta_{KSCN} + \eta_{KSCN} \times \eta_{DAM})}{1 - \eta_{DAM-KSCN}} \tag{3}$$

where  $\eta_{DAM}$ ,  $\eta_{KSCN}$  and  $\eta_{DAM-KSCN}$  are the  $\eta$  values of KSCN, DAM and DAM-KSCN ( $C_{KSCN}$  and  $C_{DAM}$  of DAM-KSCN are the same as that used in the corresponding separate situations) respectively. Generally,  $S$  value  $< 1$  indicates an antagonistic effect deriving from competitive adsorption, whereas  $S > 1$  represents a synergistic effect deriving from synergistic adsorption [23-24].

Thus, the values of  $R_s$ ,  $R_{ct}$ ,  $Y_0$ ,  $n$ ,  $C_{dl}$ ,  $\eta$  and  $S$  were obtained and shown in Table 1.

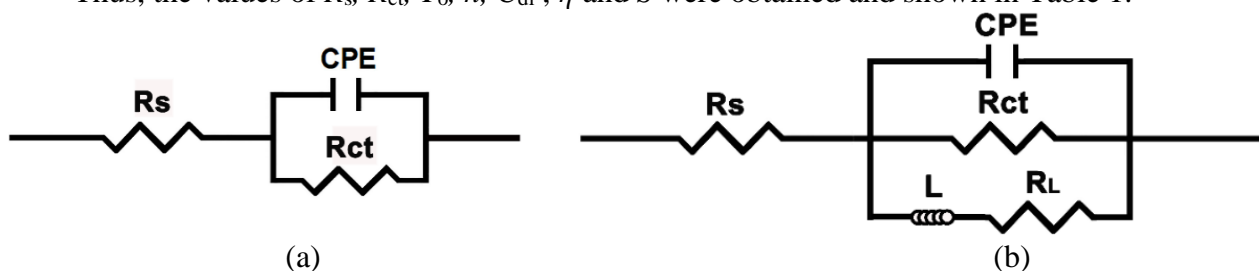


**Figure 3.** Equivalent circuit models used to simulate EIS data without (a) and with (b) inductive loop

**Table 1.** EIS parameters derived from Nyquist plots of steel in 1 M HCl solution with different concentrations of the investigated inhibitors at 303 K

$C_{DAM}$ ( $\mu\text{M}$ )	$C_{KSCN}$ (mM)	$R_s$ ( $\Omega \cdot \text{cm}^{-2}$ )	$Y_0 \times 10^6$ ( $\text{S} \cdot \text{s}^n \cdot \text{cm}^{-2}$ )	$n$	$C_{dl}$ ( $\mu\text{F} \cdot \text{cm}^{-2}$ )	$R_{ct}$ ( $\Omega \cdot \text{cm}^{-2}$ )	$L$ ( $\text{H} \cdot \text{cm}^{-2}$ )	$R_L$ ( $\Omega \cdot \text{cm}^{-2}$ )	$\eta$ (%)	$S$
0	0	1.0	220.40	0.8931	112.98	18.17	–	–	–	–
0	2	1.0	161.60	0.9092	93.22	23.16	67.27	169.3	21.5	–
5	0	0.9	173.90	0.8769	78.12	29.45	–	–	38.3	–
10	0	1.0	160.03	0.8820	71.36	41.17	–	–	55.9	–
20	0	1.1	136.20	0.8761	60.66	58.19	–	–	68.8	–

40	0	1.0	109.20	0.8720	49.93	91.65	–	–	80.2	–
80	0	1.0	72.72	0.8707	32.02	131.5	–	–	86.2	–
5	2	0.9	62.38	0.8916	33.72	105.9	996.3	908.0	82.8	2.82
10	2	0.8	42.31	0.8805	22.48	201.3	7317	2526	91.0	3.85
20	2	1.2	40.33	0.8785	22.22	303.1	–	–	94.0	4.08
40	2	0.9	38.19	0.8806	21.26	408.7	–	–	95.6	3.53
80	2	0.9	35.47	0.8717	19.37	479.1	–	–	96.2	2.85

It is evident from Table 1, the  $\eta$  value is very small and the change of  $R_{ct}$  value is slight in the single KSCN inhibitor. The  $R_{ct}$  and  $\eta$  values are distinctly increase with increasing DAM concentration while the  $C_{dl}$  values exhibit the opposite dependence in the absence of KSCN, however, when DAM concentration reach up to 80  $\mu\text{M}$  the  $\eta$  value of single DAM is still less than 90 %, implying that DAM molecules can absorb on steel surface and reduce steel corrosion while inhibition performance is modest in 1 M HCl without the addition of KSCN at 303 K.

It can be also apparently seen from Table 1, the  $R_{ct}$  and  $\eta$  values are dramatically increase with increasing DAM concentration while the  $C_{dl}$  values show the opposite dependence in presence of DAM and KSCN. It is worth noting that the  $\eta$  values of the mixed corrosion inhibitors are obviously larger than that of the single DAM inhibitor at the same DAM concentration, and the  $\eta$  value is up to 96.2 % in 80  $\mu\text{M}$  DAM and 2 mM KSCN at 303 K, hence, DAM-KSCN may be considered as an excellent inhibitor for steel corrosion. The synergistic inhibition effect between thiocyanate ions and DAM cations can be quantitatively expressed by the synergism parameters, Table 1 shows that  $S$  values are in range of 2.82 to 4.08, suggesting that the synergistic adsorption of DAM cations and thiocyanate ions may dramatically improve the surface coverage of the inhibitor molecules [23-24].

### 3.2 Potentiodynamic polarization

The polarization curves of mild steel in 1 M HCl in the absence and presence of the investigated inhibitors at 303 K are shown in Fig. 4 and Fig. 5, respectively. The corresponding parameters including the corrosion potential ( $E_{corr}$ ), the cathodic Tafel slope ( $\beta_c$ ), the anodic Tafel slope ( $\beta_a$ ), the inhibition efficiency ( $\eta$ ) and the corrosion current density ( $j_{corr}$ ) deduced from the polarization curves are summarized in Table 2. The  $\eta$  values are calculated from the following equation [25]:

$$\eta \% = \frac{(j_{corr,0} - j_{corr,i})}{j_{corr,0}} \times 100 \% \quad (4)$$

where  $j_{corr,0}$  and  $j_{corr,i}$  are the  $j_{corr}$  values in the absence and presence of the investigated inhibitor respectively.

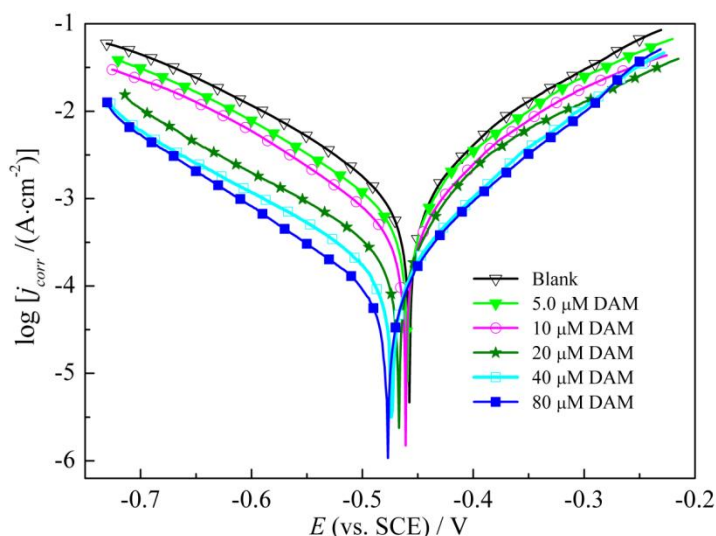


**Figure 4.** Polarization curves of mild steel in 1 M HCl with different concentrations of DAM at 303 K

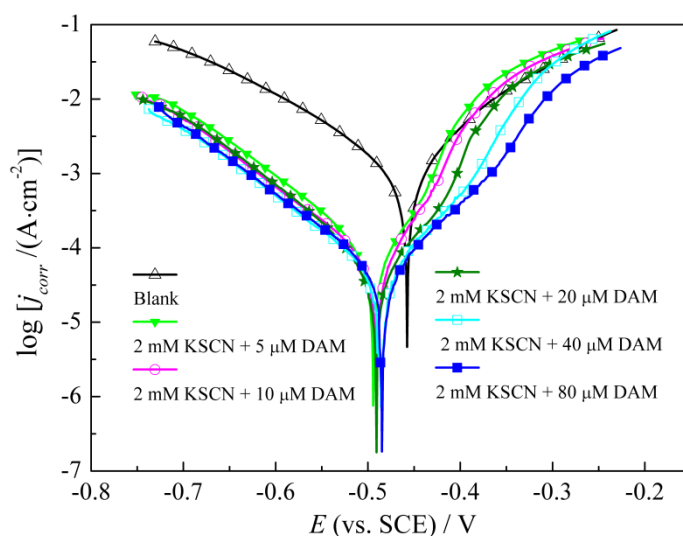


**Figure 5.** Polarization curves of mild steel in 1 M HCl and 2 mM KSCN with different concentrations of DAM at 303 K

**Table 2.** Potentiodynamic parameters for the corrosion of mild steel in 1 M HCl solution with different concentrations of the investigated inhibitors at 303 K.

$C_{DAM}$ ( $\mu\text{M}$ )	$C_{KSCN}$ (mM)	$E_{corr}$ (V vs SCE)	$j_{corr}$ ( $\text{mA}\cdot\text{cm}^{-2}$ )	$\beta_c$ ( $\text{mV}\cdot\text{dec}^{-1}$ )	$\beta_a$ ( $\text{mV}\cdot\text{dec}^{-1}$ )	$\eta$ (%)
0	0	-0.458	1061.19	121	87	—
5	0	-0.459	628.79	120	82	40.7
10	0	-0.461	508.85	116	91	52.0
20	0	-0.467	344.57	136	93	67.5

40	0	-0.474	204.28	138	89	80.7
80	0	-0.477	95.55	118	88	91.0
5	2	-0.494	92.18	105	81	91.3
10	2	-0.491	71.53	113	73	93.3
20	2	-0.491	57.72	100	88	94.6
40	2	-0.486	42.94	106	78	96.0
80	2	-0.485	37.72	113	94	96.4

As can be clearly seen from Fig. 4 and Table 2, the cathodic and anodic current curves in the presence of the single DAM inhibitor both decrease and the  $\eta$  values increase with increasing DAM concentration, in addition,  $\beta_c$  and  $\beta_a$  values do not change remarkably and the corrosion potentials shift slightly to negative values in comparison with the observed results in blank solution, indicating that DAM is a representative mixed-type inhibitor and may simultaneously retard anodic dissolution of metals as well as restrain cathodic hydrogen evolution reaction without significant change of corrosion mechanism only by simple adsorption mode on steel surface [26].

Inspection of Fig. 5 and Table 2, the cathodic and anodic curves dramatically shift to lower current densities with increasing DAM concentration in the presence of 2 mM KSCN, and the inhibition efficiencies of DAM-KSCN are significantly higher than that of DAM alone in the same DAM concentration, confirming again that DAM-KSCN is an excellent inhibitor for steel corrosion in 1 M HCl solution. Similar to DAM inhibitor, the corrosion potentials of DAM-KSCN inhibitor increase with increasing DAM concentration, but these corrosion potentials are more negative than that of DAM alone, hinting that the addition of KSCN may reduce the corrosion potential. All corrosion potential in the presence of DAM-KSCN are lower than that in blank solution while the  $E_{\text{corr}}$  displacement is less than 85 mV, indicating that DAM-KSCN can be seen as a mixed-type inhibitor dominantly controlled by cathodic reaction. Fig. 5 shows that the anodic polarization curves do not display a typical Tafel region, which should be due to the desorption of inhibitor molecules on steel surface relating to the absorption stability of DAM molecules,  $\text{SCN}^-$  and other ions. However, the anodic desorption degree of DAM-KSCN can gradually decrease with increasing DAM concentration. In this case,  $j_{\text{corr}}$  and  $\beta_a$  values may be obtained by the extrapolation of the cathodic Tafel region below the corrosion potential [27-29], and the obtained results were given in Table 2. Table 2 shows the cathodic branch of polarization curves of DAM-KSCN are almost coincident and  $\beta_c$  and  $\beta_c$  values of these curves both are slightly less than that in blank solution, suggesting that the change of the corrosion mechanism of the anodic and the cathodic reactions is slight.

### 3.3. Weight loss

The weight loss measure is an effective and traditional method to assess inhibition performance. Table 3 shows the weight loss results of mild steel in 1.0 M HCl solution in the absence

and presence of the investigated inhibitor for 6 h at various temperatures. The corrosion rate ( $v$ ), the inhibition efficiency ( $\eta$ ) and the surface coverage ( $\theta$ ) may be calculated as follows [30]:

$$v = \frac{w}{A \cdot t} \quad (5)$$

$$\eta (\%) = \frac{(v_0 - v_i)}{v_0} \times 100 \% \quad (6)$$

$$\theta = \frac{\eta}{100} \quad (7)$$

Where,  $w$  is the weight loss of steel coupon,  $A$  is the total surface area of steel coupon,  $t$  is the immersion time,  $v_0$  and  $v_i$  are the values of the corrosion rate in the absence and presence of the investigated inhibitors respectively.

**Table 3.** The weight loss results of mild steel in 1.0 M HCl with various concentrations of the investigated inhibitors at different temperatures

$T$ (K)	Inhibitor concentration		$V$ ( $\text{g} \cdot \text{m}^{-2} \cdot \text{h}^{-1}$ )	$\eta$ (%)	$\theta$
	DAM ( $\mu\text{M}$ )	KSCN (mM)			
303	0	0	10.16	–	–
	5	0	4.44	56.3	0.563
	10	0	3.18	68.7	0.687
	20	0	2.33	77.1	0.771
	40	0	1.60	84.3	0.843
	80	0	0.98	90.4	0.904
	5	2	0.77	92.4	0.924
	10	2	0.62	93.9	0.939
	20	2	0.52	94.9	0.949
	40	2	0.49	95.2	0.952
313	0	0	20.50	–	–
	80	0	3.40	83.4	0.834
	80	2	0.83	96.0	0.960
323	0	0	37.95	–	–
	80	0	9.04	76.2	0.762
	80	2	1.89	95.0	0.950

As shown in Table 3, the corrosion rate decreases and the  $\eta$  value increases with increasing DAM concentration in the absence and presence of 2 mM KSCN respectively at 303 K, and the change tendency of the  $\eta$  value is in good correspondence with the test results of EIS and polarization, confirming again that DAM molecules can absorb on steel surface to reduce steel corrosion in 1.0 M

HCl at 303 K and the inhibition performance of DAM can further improve by the addition of KSCN. Furthermore, the inhibition efficiency of DAM alone obviously decreases with the increase of temperature while temperature has almost no influence on the  $\eta$  value of DAM-KSCN at the temperature range of 303-323K, hinting that the synergistic advantage of DAM and KSCN may further improve at higher temperature within a certain temperature range [31].

### 3.4 Adsorption isotherm and thermodynamic parameters

To accurately exhibits the interaction process between the investigated inhibitors and steel surface, a series of adsorption isotherms were applied to fit the weight loss results at 303 K. As a result, Langmuir adsorption isotherm was found to be the most appropriate model. Langmuir adsorption isotherm and thermodynamic parameters may be calculated according to the following equations [32]:

$$\frac{C}{\theta} = \frac{1}{K_{\text{ads}}} + C \quad (8)$$

$$\Delta G_{\text{ads}}^0 = -RT \ln(55.5 K_{\text{ads}}) \quad (9)$$

where,  $C$  is the inhibitor concentration,  $\theta$  comes from weight loss test,  $K_{\text{ads}}$  is the adsorption equilibrium constant,  $\Delta G_{\text{ads}}^0$  is the standard free energy of adsorption and  $R$  is the universal gas constant.

Consequently, the plots of  $C$  versus  $C/\theta$  may be given in Fig. 6.

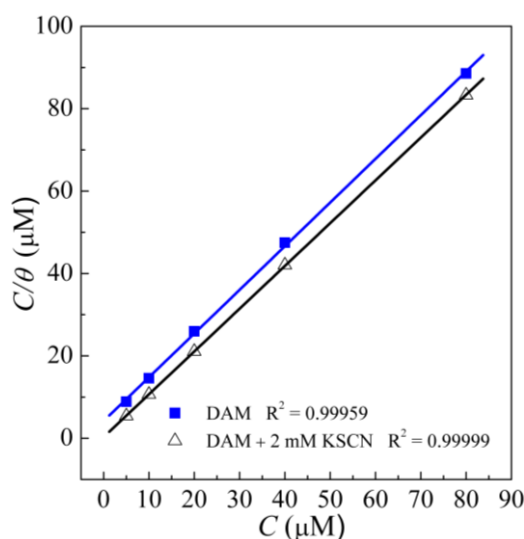


**Figure 6.** Langmuir isotherm plots in 1.0 M HCl with various concentrations of DAM in the absence and the presence of KSCN

As shown in Fig. 6, each plot of  $C$  versus  $C/\theta$  yield a straight line at 303 K and the correlation coefficients ( $R^2$ ) and the slope both are near 1, indicating that Langmuir adsorption isotherm is appropriate for data fitting [32].

The calculated results show that the  $\Delta G_{ads}^0$  values are - 41 and - 48  $\text{KJ}\cdot\text{mol}^{-1}$  for DAM and DAM-KSCN respectively, implying that the adsorption mechanism of DAM and DAM-KSCN on steel surface both are chemical adsorption [32-33]. The  $\Delta G_{ads}^0$  value of DAM-KSCN is more negative than that of DAM, suggesting that DAM-KSCN has stronger interaction with steel surface than single DAM [34]. Undoubtedly, KSCN plays an important role in enhancing the absorption of DAM molecule on steel surface.

### 3.5. Kinetic parameters

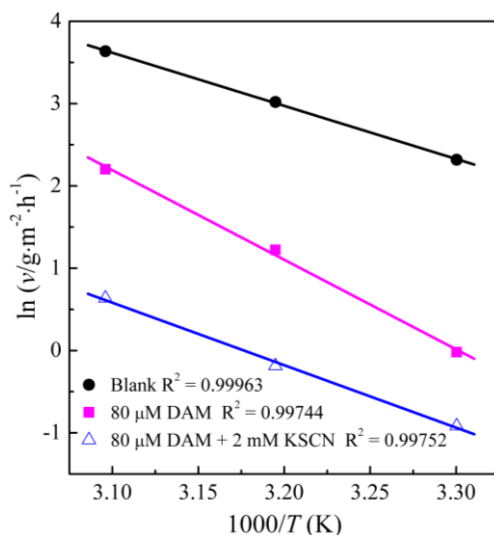


**Figure 7.** Arrhenius plots for mild steel in 1.0 M HCl without and with the investigated inhibitors

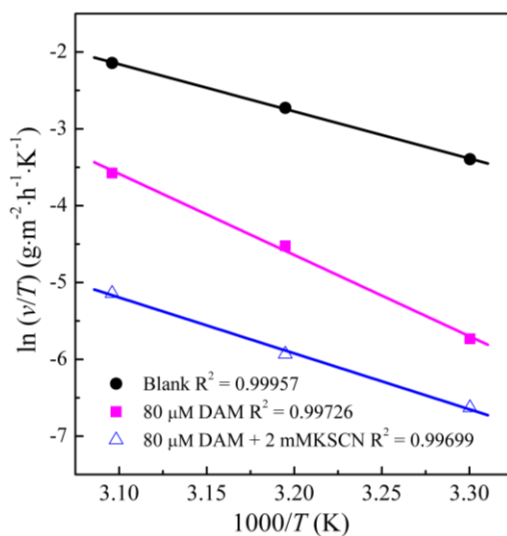


**Figure 8.** Transition state plots for mild steel in 1.0 M HCl without and with the investigated inhibitors

To obtain and evaluate adsorption kinetic parameters of the investigate inhibitors, the effect of temperature on the corrosion rate in 1.0 M HCl solution was studied using Arrhenius and Transition state equations[34]:

$$\ln v = -\frac{E_a}{RT} + \ln \lambda \quad (10)$$

$$\ln v/T = \ln \frac{R}{Nh} + \frac{\Delta S_a}{R} - \frac{\Delta H_a}{RT} \quad (11)$$

where,  $\lambda$  is the pre-exponential factor,  $h$  is the plank's constant,  $N$  is Avogadro's number,  $E_a$  is the apparent activation energy,  $\Delta S_a$  is the apparent entropy of activation,  $\Delta H_a$  is the apparent enthalpy of activation.

Thus, Arrhenius plots and Transition state plots may be obtained and shown in Fig. 7 and Fig. 8, respectively.

Obviously, the  $R^2$  values of the fitting straight lines in Fig. 7 and 8 are close to one in all cases. Consequence, the adsorption kinetic parameters such as  $E_a$ ,  $\Delta H_a$  and  $\Delta S$  are obtained from equation 11 and 12 and listed in Table 4,  $\Delta S$  may be calculated according to the following equations [7].

$$\Delta S = \Delta S_{a,i} - \Delta S_{a,0} \quad (12)$$

where,  $\Delta S_{a,0}$  and  $\Delta S_{a,i}$  is the  $\Delta S_a$  values in the absence and presence of the investigated inhibitor respectively.

**Table 4.** Kinetic parameters for mild steel in 1.0 M HCl without and with the investigated inhibitors

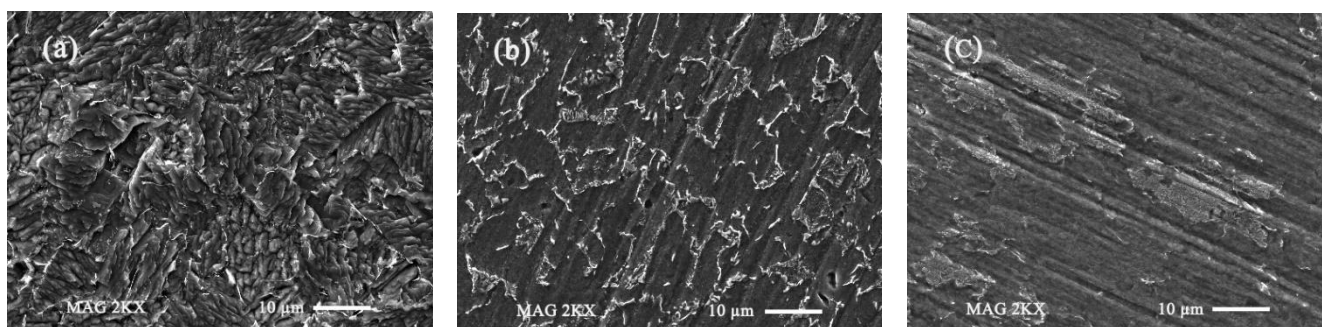
Inhibitor concentration		$E_a$ (kJ·mol <sup>-1</sup> )	$\Delta H_a$ (kJ·mol <sup>-1</sup> )	$\Delta S$ (J·mol <sup>-1</sup> ·K <sup>-1</sup> )
DAM ( $\mu$ M)	KSCN (mM)			
0	0	54	51	–
80	0	90	88	102
80	2	63	61	4

Table 4 shows that the  $E_a$  values of DAM alone is are significantly greater than that in blank solution, clearly, DAM molecules may protect steel surface by improving energy barrier of the corrosion process associated with weak chemical adsorption in acid medium. Whereas the  $E_a$  values of DAM-KSCN is only slightly greater than that in blank solution, indicating that DAM-KSCN may more firmly attach to steel surface to inhibit steel corrosion by the stronger chemical adsorption than DAM alone, which is in accordance with the difference of the  $\Delta G_{ads}^0$  values [35-36]. Therefore, the inhibition efficiency of DAM-KSCN is more stable with the increase of the temperature than that of DAM alone at 303 - 323K. In addition, the  $\Delta H_a$  values in any case are positive signifying the endothermic nature of steel dissolution process in acid medium. Based on the well-known thermodynamic equation:  $\Delta H_a = E_a - RT$ , it's easy to explain that the  $\Delta H_a$  values exhibit the same change trend as the  $E_a$  values [35]. Inspection of Table 4, the  $\Delta S$  values in DAM-KSCN solution are greater than zero and increase further in single DAM solution, hinting that the addition of the two inhibitors can result in the increase of the

disorder degree during the formation of the activated complex in the corrosion process, and the disorder degree of DAM alone may reduce with the addition of 2 mM KSCN [36].

### 3.6 Surface characterization

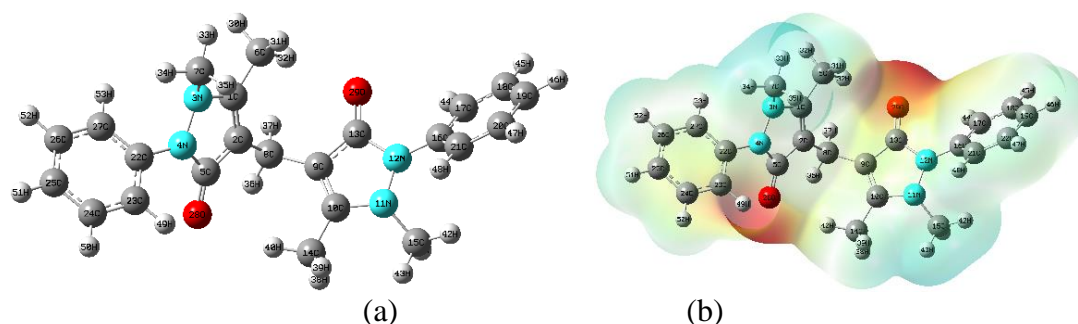
To directly evaluate the morphology change of steel surface during corrosion process, SEM tests of steel panels was performed after 4 h of immersion in investigated solution at 303 K and the micrographs are given in Fig. 9. The steel surface in blank solution is badly damaged with cracks and pits because steel surface was severely corroded by the aggressive acid without the protection of any inhibitor. Nevertheless, the damage of the steel surface is considerably decreased after addition DAM alone. Furthermore, the damage of the steel surface in the presence of DAM-KSCN is further reduced and exhibits a relatively smooth surface, which indicates that the results of the micrographs are in accordance with the inhibition performance obtained from the results weight loss and electrochemical tests.



**Figure 9.** SEM micrographs of mild steel surface after 4 h immersion at 303K:1.0 M HCl solution (a), 1.0 M HCl + 80  $\mu$ M DAM (b) and 1.0 M HCl + 80  $\mu$ M DAM + 2.0 mM KSCN (c)

### 3.7 Quantum chemical calculations

The quantum chemical investigations were employed to further understand the structure-activity relationships of DAM molecule in aqueous phase. Consequently, the optimized plots including the electrostatic potential map (ESP, the red and blue regions represent negative and positive, respectively), the distributions of HOMO and the distributions of LUMO are given in Fig. 10, and the corresponding parameters are listed in Table 5 respectively.



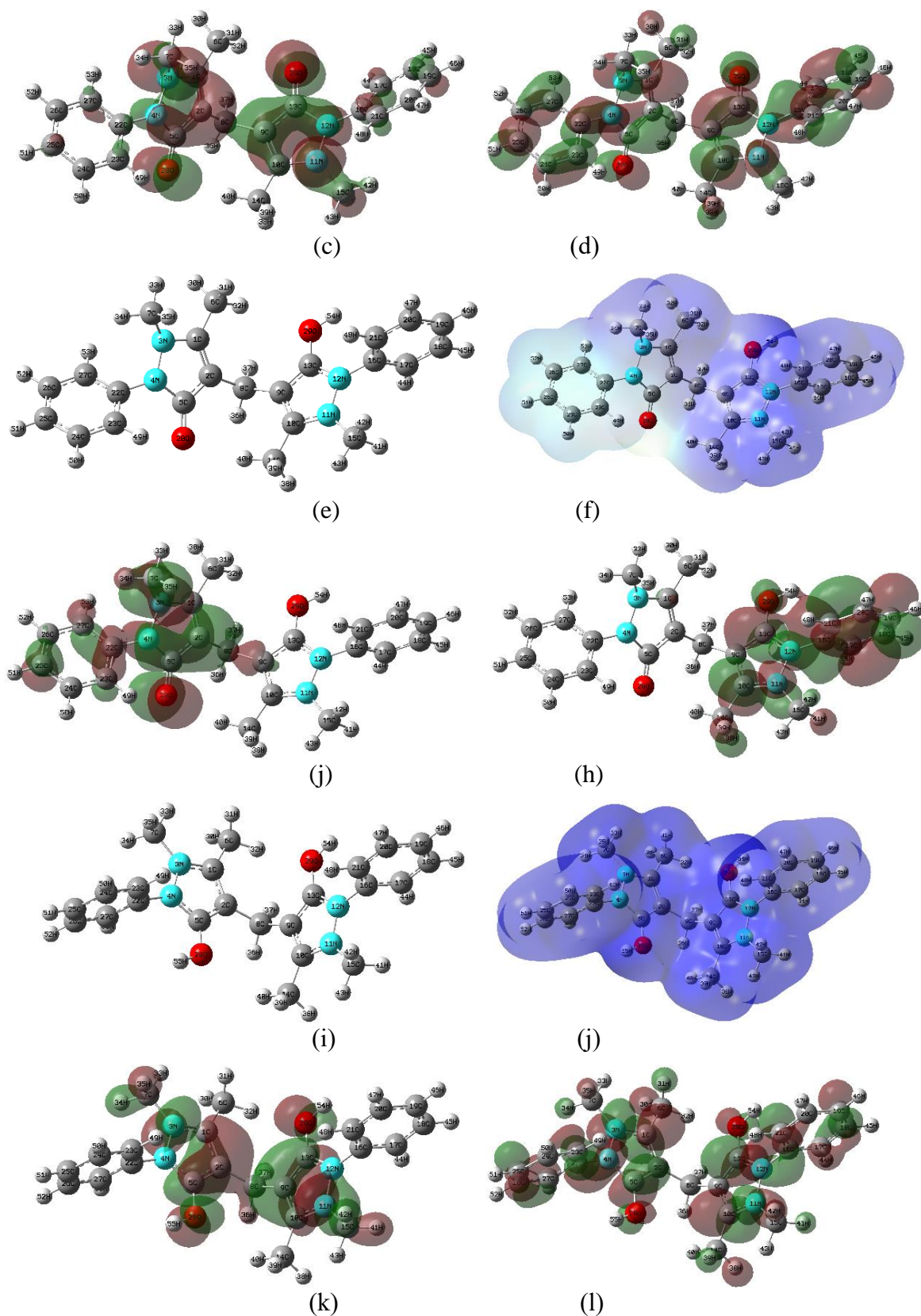


**Figure 10.** The obtained plots coming from quantum chemical calculation in aqueous phase: the optimized geometries of DAM (a), DAMH<sup>+</sup> (e) and DAMH<sub>2</sub><sup>2+</sup> (i), the ESP images of DAM (b), DAMH<sup>+</sup> (f) and DAMH<sub>2</sub><sup>2+</sup> (j), the HOMO distributions of DAM (c), DAMH<sup>+</sup> (g) and DAMH<sub>2</sub><sup>2+</sup> (k) and the LUMO distributions of DAM (d), DAMH<sup>+</sup> (h) and DAMH<sub>2</sub><sup>2+</sup> (l)

**Table 5.** Quantum chemical parameters for DAM, DAMH<sup>+</sup> and DAMH<sub>2</sub><sup>2+</sup>

DAM forms	$E_{\text{HOMO}}$ (ev)	$E_{\text{LUMO}}$ (ev)	$\Delta E$ (ev)	$\mu$ (D)	Total Energy (ev)
DAM	-5.606	-0.782	4.824	5.675	-34286.336
DAMH <sup>+</sup>	-5.809	-1.228	4.581	16.328	-34298.298
DAMH <sub>2</sub> <sup>2+</sup>	-7.275	-1.348	5.927	0.261	-34310.167

The red (negative) and blue (positive) of the ESP maps are related to nucleophilic and electrophilic activities, respectively. Obviously, the net charge of various forms of DAM can affect the molecular structure, the ESP images and the distributions of HOMO and LUMO. As evidenced in Fig. 10, the red region concentrate on the surfaces of two oxygen atoms in the ESP image of the neutral form of DAM, whereas the most region of the ESP image of DAMH<sup>+</sup> and the complete region of the ESP image of DAMH<sub>2</sub><sup>2+</sup> exhibit the dark blue, suggesting that the nucleophilic activity from high to low is DAM, DAMH<sup>+</sup> and DAMH<sub>2</sub><sup>2+</sup> while the electrophilic activity exhibits the opposite tendency [37], which are consistent with the change tendencies of the values of  $E_{\text{HOMO}}$  and  $E_{\text{LUMO}}$  in table 5. In addition, the HOMO and LUMO of DAM and DAMH<sub>2</sub><sup>2+</sup> exhibit symmetrical distribution while the HOMO of DAMH<sup>+</sup> locates in one side and its LUMO locates in the other side, which are agree with the symmetry of the molecular structure.

As shown in Table 5, the total energy from high to low is DAM, DAMH<sup>+</sup> and DAMH<sub>2</sub><sup>2+</sup>, hinting that the dication structure is the major form in the equilibrium of the different forms of DAM in aqueous phase [38].

Based on the frontier molecular orbital theory, the HOMO is associated with the electron donating capacity of inhibitor molecules while the LUMO represents the electron accepting ability. In general, the higher value of  $E_{\text{HOMO}}$ , the lower value of  $E_{\text{LUMO}}$  and the lower value of  $\Delta E$  of inhibitor molecule may exhibit the more excellent inhibition performance [37-38]. As can be seen in Fig. 10, the optimized structure and the distributions of HOMO and LUMO within DAM<sup>2+</sup> molecule are symmetric. HOMO mainly located in two pyrazolone rings and two oxygen atoms while LOMO distribute all over the entire region of DAM<sup>2+</sup> molecule except the central atom of the symmetric molecule. It is obvious that DAMH<sub>2</sub><sup>2+</sup> with the dication structure and the low  $E_{\text{HOMO}}$  value can hardly adsorb on steel surface by donating electrons of two pyrazolone rings and two oxygen atoms, however, the electron-deficient regions of DAMH<sub>2</sub><sup>2+</sup> molecules are beneficial to the absorption of DAM<sup>2+</sup> molecule on steel surface in acid medium by accepting the d orbital electrons of metal atoms such as iron atoms or the bridging action of Cl<sup>-</sup> or SCN<sup>-</sup> [39-40].

#### 4. CONCLUSION

The inhibition performance of DAM and its synergistic effect with KSCN on mild steel corrosion in 1.0 M HCl solution have been investigated. It can be concluded as follows:

(1) DAM is a modest inhibitor for mild steel corrosion in 1.0 M HCl solution but the inhibition performance can obviously be enhanced with the addition of KSCN by the bridging action of  $\text{SCN}^-$ .

(2) The inhibition efficiency of DAM decreases sharply whereas that of DAM-KSCN is nearly invariable with increasing temperature at 303 - 323K.

(3) DAM and DAM-KSCN both are mixed type inhibitors by chemical adsorption and follow Langmuir adsorption model on steel surface.

(4) Theoretical calculation shows that DAM inhibits steel corrosion in aqueous phase by the adsorption of  $\text{DAM}^{2+}$  molecules on the steel surface.

#### ACKNOWLEDGEMENT

This project is supported by Natural Science Foundation of China (No. 51502182).

#### References

1. A.A. Olajire, *J. Mol. Liq.*, 248 (2017) 775.
2. M. Goyal, S. Kumar, I. Bahadur, C. Verma and E.E. Ebenso, *J. Mol. Liq.*, 256(2018) 565.
3. M. Mandavian, A.R. Tehrani-Bagha, E. Alibakhshi, S. Ashhari, M.J. Palimi, S. Farashi, S. Javadian and F. Ektefa, *Corros. Sci.*, 137(2018) 62.
4. M.A. Micahed and I.F. Nassar, *Electrochim. Acta.*, 53 (2008) 2877.
5. Q. Ma, S.J. Qi, X.H. He, Y.M. Tang and G. Lu, *Corros. Sci.*, 129(2017) 91.
6. M. Finsgar and J. Jackson, *Corros. Sci.*, 86(2014) 17.
7. L.J. Gong and K.Q. Qiao, *Int. J. Electrochem. Sci.*, 11(2016) 10135.
8. A.S. Fouda, S.A. El-Sayyad and M. Abdallah, *Anti-corros. Method. M.*, 58 (2011) 63.
9. E. Khamis, E.S.H. El-Ashry and A.K. Ibrahim, *Brit. Corros. J.*, 35 (2000) 150.
10. A.S. Fouda, G.Y. Elewady and A.M. Abdel-Fattah, *Prot. Met. Phys. Chem.*, 47 (2011) 253.
11. A.S. Fouda, M. Abdallah and A. Attia, *Chem. Eng. Commun.*, 197 (2010) 1091.
12. A.S. Fouda, A.A. Al-Sarawy and E.E. El-Katori, *Desalination.*, 201 (2006) 1.
13. C. Verma, M.A. Quraishi, E.E. Ebenso, I.B. Obot and A. El Assyry, *J. Mol. Liq.*, 219(2016) 647.
14. M. Outirite, M. Lagrenee, M. Lebrini, M. Traisnel, C. Jama, H. Vezin and F. Bentiss., *Electrochim. Acta.*, 55 (2010) 1670.
15. A.A. Farag and T.A. Ali, *J. Ind. Eng. Chem.* 21 (2015) 627.
16. A. Fitoz, H. Nazir, M. Ozgur, E. Emregul and K.C. Emregul, *Corros. Sci.*, 133 (2018) 451.
17. G. Sigircik, D. Yildirim and T. Tuken, *Corros. Sci.*, 120 (2017)184.
18. A. Yousefi, S. Javadian and J.Neshati, *J. Ind. Eng. Chem.* 53 (2014) 5475.
19. Z.Y. Hu, Y.B. Meng, X.M. Ma, H.L. Zhu, J. Li, C.Li and D.L. Cao, *Corros. Sci.*, 112 (2015) 563.
20. R.Salghi, S.Jodeh, E.E. Ebenso, H. Lgaz, D. Ben Hmamou, I.H. Ali, M. Messali, B. Hammouti and N. Benchat, *Int. J. Electrochem. Sci.*, 12(2017) 3309.
21. D.K. Singh, S.Kumar, G.Udayabhanu and R.P. John, *J. Mol. Liq.*, 216(2016) 738.
22. A. Singh, K.R. Ansari, M.A. Quraishi, H. Lgaz and Y.H. Lin, *J. Alloy. Compd.*, 762 (2018) 347.
23. P. Han, C.F. Chen, W.H. Li, H.B. Yu, Y.Z. Xu, L. Ma and Y.J. Zheng, *J. Colloid. interf. Sci.*, 516(2018) 398.
24. A. Khamis, M.M. Saleh, M.I. Awad and B.E. El-Anadouli, *Corros. Sci.*, 74 (2013)83.
25. H. Rahmani, K.I. Alaoui, K.M. Emran, A. El Hallaoui, M. Taleb, S. El Hajji, B. Labriti, E. Ech-Chihbi, B. Hammouti and F. El-Hajjaji, *Int. J. Electrochem. Sci.*, 14(2019) 985.
26. P. Arellanes-Lozada, O. Olivares-Xometl, N.V. Likhanova, I.V. Lijanova, J.R. Vargas-Garcia and R.E. Hernandez-Ramirez, *J. Mol. Liq.*, 265(2018)151.
27. E. McCafferty, *Corros. Sci.*, 47 (2005) 3202.
28. M.A. Amin, K.F. Khaled and S.A. Fadel-Allah., *Corros. Sci.*, 52 (2010) 140.

29. K.F. Khaled and M.A. Amin, *Corros. Sci.*, 51 (2009) 1964.
30. X.Y. Zhang, Y.X. Zheng, X.P. Wang, Y.F. Yan and W. Wu, *J. Ind. Eng. Chem.* 53 (2014) 14199.
31. S. Merah, L. Larabi, O. Benali and Y. Harek, *Pigm. Resin. Technol.*, 37(2008) 291.
32. N. Kicir, G. Tansug, M. Erbil and T. Tuken, *Corros. Sci.*, 105 (2016) 88.
33. A. Fawzy, I.A. Zaafarany, H.M. Ali and M. Abdallah, *Int. J. Electrochem. Sci.*, 13(2018) 4575.
34. C. Wang, J.X. Chen, J. Han, C.B. Wang and B.S. Hu, *J. Alloy. Compd.*, 771 (2019) 736.
35. M.M. Solomon and S.A. Umoren, *J. Environ. Chem. Eng.*, 3 (2015) 1812.
36. K. Ramya, R. Mohan, K.K. Anupama and A. Joseph, *Mater. Chem. Phys.*, 149 (2015) 632.
37. L. Feng, S.T. Zhang, Y.J. Qiang, S.Y. Xu, B.C. Tan and S.J. Chen, *Mater. Chem. Phys.*, 215 (2018)229.
38. I. Danaee, M. Gholami, M. RashvandAvei and M.H. Maddahy, *J. Ind. Eng. Chem.*, 26 (2015) 81.
39. A. Singh, K.R. Ansari, M.A. Quraishi, H. Lgaz and Y.H. Lin., *J. Alloy. Compd.*, 762 (2018) 347.
40. S.M. Shaban, A.S. Fouda, S.M. Rashwan, H.E. Ibrahim and M.F. Elbhrawy, *Prot. Met. Phys. Chem.*, 54 (2018) 709.

© 2019 The Authors. Published by ESG ([www.electrochemsci.org](http://www.electrochemsci.org)). This article is an open access article distributed under the terms and conditions of the Creative Commons Attribution license (<http://creativecommons.org/licenses/by/4.0/>).